

[Click here to view linked References](#)

1  
2 **Waste Composition-Dependent “HBM” Model Parameters Based on Degradation**  
3 **Experiments**  
4

5  
6 Author 1

- 7  
8
  - Sampurna Datta, PhD Candidate
  - Department of Civil and Environmental Engineering, University of Michigan, Ann Arbor,  
9 United States

10  
11

12 Author 2

- 13  
14
  - Dimitrios Zekkos, Associate Professor
  - Department of Civil and Environmental Engineering, University of Michigan, Ann Arbor,  
15 United States

16  
17

18 Author 3

- 19  
20
  - Xunchang Fei, Assistant Professor
  - Department of Civil and Environmental Engineering, Nanyang Technological University,  
21 Singapore

22  
23

24 Author 4

- 25  
26
  - John McDougall, Reader
  - School of Engineering and the Built Environment, Edinburgh Napier University, Edinburgh,  
27 United Kingdom

28  
29  
30

31  
32 **Corresponding author contact: sampurna@umich.edu**  
33

34  
35  
36 This manuscript is revised on September 5, 2018. It contains 4,333 words in the main text and  
37 422 words in tables (4 tables) and 6 figures.  
38  
39  
40  
41  
42  
43  
44  
45  
46  
47  
48  
49  
50  
51  
52  
53  
54  
55  
56  
57  
58  
59  
60  
61  
62  
63  
64  
65

## Abstract

Municipal solid waste (MSW) is biodegradable in landfills under anaerobic conditions. The evolution of the hydro-biochemical-mechanical (HBM) processes during degradation is investigated first through experiments and subsequently via modelling. Three well-characterized MSW specimens with significantly different waste composition ranging from “waste-rich” to “soil-rich” were degraded in large-scale experimental setups that enabled simultaneous characterization of the processes with time. The closely-monitored processes are subsequently modelled using a two-stage anaerobic degradation model which is incorporated in the HBM model. This allows an assessment of model performance as a function of waste composition and derivation of waste composition-dependent model parameters. The model performed fairly well in capturing the biochemical and physical behaviour. An increase in biodegradable material in waste specimen corresponds to increase in anaerobic activity (volatile fatty acids and methanogenic biomass accumulation), higher rate of organic fraction depletion, increase in settlement and increase in methane production. However, the model is found to significantly over-predict methane production for all the specimens.

## Keywords chosen from ICE Publishing list

Environmental Engineering; Energy; Geochemistry

## List of notations

$B_0$	is the percentage of biodegradable waste
$\gamma_{d,l}$	is the dry unit weight of the specimen after immediate compression was practically completed in $\text{kg.m}^{-3}$
$\gamma_{B,l}$	is the density of biodegradable waste in $\text{kg.m}^{-3}$
$c$	is the VFA concentration in aqueous medium in $\text{g.m}^{-3}$
$m$	is the methanogen biomass (MB) in aqueous medium in $\text{g.m}^{-3}$
$r_g$	is the rate of VFA accumulation in $\text{g VFA.m}^{-3} \text{aqueous.day}^{-1}$
$\theta_E$	is the effective volumetric moisture content
$b$	is the maximum VFA growth rate in $\text{g.m}^{-3} \text{aqueous.day}^{-1}$
$S$	is the solid degradable fraction in $\text{g.m}^{-3}$
$n$	is the structural transformation parameter
$\phi$	is the relative digestibility of solid degradable fraction
$k_{VFA}$	is the product inhibition constant in $\text{g.m}^{-3}$
$P$	is the inhibition factor accounting for the inhibitory effect of high VFA concentration
$k_0$	is the maximum specific growth rate for cellulose in $\text{day}^{-1}$
$k_{MC}$	is the half saturation constant in $\text{g.m}^{-3}$
$r_j$	is the methanogenic biomass production rate in $\text{g.m}^{-3} \text{.day}^{-1}$

1	$Y$	is the cell/substrate yield coefficient
2	$k_2$	is the methanogen death rate in $\text{day}^{-1}$
3	$r_k$	is the methanogenic biomass decay rate in $\text{g.m}^{-3}.\text{day}^{-1}$
4		
5	$\rho_{H_2O}$	is the density of water in $\text{kg.m}^{-3}$
6		
7	$V_s$	is the solid phase volume
8	$V_v$	is the void volume
9		
10	$\Lambda$	is the decomposition (or degradation)-induced void change parameter
11	$e$	is the void ratio
12		
13	$\chi$	is the creep viscosity coefficient
14	$t_{eq}$	is the equivalent time in days
15		
16	$t_{ref}$	is the reference time in days
17		
18		
19		
20		
21		
22		
23		
24		
25		
26		
27		
28		
29		
30		
31		
32		
33		
34		
35		
36		
37		
38		
39		
40		
41		
42		
43		
44		
45		
46		
47		
48		
49		
50		
51		
52		
53		
54		
55		
56		
57		
58		
59		
60		
61		
62		
63		
64		
65		

1 **1. Introduction**

2 Approximately 53% of the municipal solid waste (MSW) generated in the U.S. is disposed of in  
3 sanitary landfills (US EPA, 2014). The solid, liquid and gas phases of MSW in a landfill evolve  
4 with time due to coupled physical-biochemical-mechanical and hydraulic processes during  
5 anaerobic biodegradation (Fei and Zekkos, 2018). Under appropriate conditions, anaerobic  
6 microorganisms consume the biodegradable organic fractions including food waste, yard waste,  
7 paper and other organics eventually converting them to biogas. The process begins with  
8 bacterial hydrolysis of the complex organic waste into simpler forms, leading to mass loss and  
9 void creation in the waste matrix. As a consequence, physical properties, such as porosity and  
10 unit weight, change. Hydrolysis results in the dissolution of organic compounds in the leachate  
11 and is followed by acidogenesis and methanogenesis which produces biogas consisting  
12 primarily of methane and carbon dioxide (Barlaz et al., 2010). As a result, the phase  
13 relationships between solid, liquid and gas phases within the MSW matrix are altered. In order  
14 to understand, predict, and possibly control waste decomposition in sanitary landfills, one must  
15 first understand the anaerobic process of degradation occurring in the waste matrix. Batstone et  
16 al. (2002) developed a structured model, ADM1, including multiple steps describing biochemical  
17 as well as physicochemical processes in anaerobic digestion. Machado et al. (2008) developed  
18 a numerical model that incorporated the biodegradation of organic matter in landfilled MSW.  
19 Gawande et al. (2010) presented a numerical model, BIOKEMOD-3P, to investigate the  
20 biochemical processes with multi-phase systems that take place in bioreactor landfills. Chakma  
21 et al. (2016) developed a mathematical model to compute the chemical compositions of the  
22 organic portion of MSW.

23  
24 Datta et al. (2017) studied the coupled degradation process and its evolution through numerical  
25 modelling of one MSW specimen with a unique composition. A biodegradation model was used  
26 to describe the anaerobic process and account for hydrolysis of degradable matter in relation to  
27 moisture content, product inhibition, cellulose digestibility and microbial controls. In this study,  
28 however, three significantly different waste compositions have been investigated in large-scale  
29 experimental setups and a two-stage anaerobic model was implemented and calibrated with the  
30 experiments. Specifically, the biodegradation component in the hydro-bio-mechanical (HBM)

1 31 formulation described by McDougall (2007) is adopted here to describe the hydrolysis,  
2 32 acidogenesis and methanogenesis reactions. The HBM model provides a constitutive  
3  
4 33 framework for the integrated analysis of the hydraulic, biodegradation and mechanical  
5  
6 34 behaviour of landfilled waste. HBM comprises three main component models that are coupled  
7  
8 35 through link routines and continually updated to ensure each component model and its influence  
9  
10 36 over others evolves during the simulation. The biodegradation component of the HBM model  
11  
12 37 which is the focus of this study neglects the aerobic stage since the aerobic waste  
13  
14 38 decomposition represents a minor part of the landfill lifetime and is considered less significant  
15  
16 39 than anaerobic decomposition in terms of organic conversion. The outcome of this modelling  
17  
18 40 effort is the derivation of model parameters that match the experimental data as a function of  
19  
20 41 waste composition. In addition, limitations to the current formulation are identified.  
21  
22 42

## 24 43 **2. Experimental Setup**

### 26 44 27 45 **2.1 Waste Characterization**

28  
29 46  
30  
31 47 The MSW specimens used in this study were collected from Austin Community Landfill in Texas  
32  
33 48 (TX), Los Reales Landfill in Arizona (AZ) and Lamb Canyon Landfill in California (CA) and  
34  
35 49 transported in sealed drums to the laboratory. Field composition was characterized according to  
36  
37 50 the procedure described by Zekkos et al. (2010). The waste was segregated into finer and  
38  
39 51 coarser fraction using a 20-mm sieve. The <20 mm fraction of each sample was soil-like. The  
40  
41 52 >20 mm fraction was manually segregated based on waste constituent type. The three primary  
42  
43 53 constituents by weight for all samples were paper, soft plastic and wood. Other minor  
44  
45 54 constituents included hard plastic, metal, rock and miscellaneous objects. No distinguishable  
46  
47 55 food waste was found in any sample. The segregated waste constituents from each sample  
48  
49 56 were weighed and the corresponding percentages on a wet weight basis were calculated. The  
50  
51 57 moisture content on a dry weight basis of the three primary >20 mm constituents and <20 mm  
52  
53 58 fraction of each sample was measured by heating the material at 70°C. The content of volatile  
54  
55 59 solids (VS) of each dried waste constituent was evaluated by heating the 70°C-dried waste at  
56  
57  
58  
59  
60  
61  
62  
63  
64  
65

60 550°C. The biodegradability of each specimen prior to degradation is evaluated using density of  
61 biodegradable waste ( $\gamma_{B,I}$ ) (Fei, 2016) defined by equations 1 and 2.

$$62 \quad B_0(\%) = \frac{\text{Dry mass of food, yard waste, paper and mass of VS in } < 20 \text{ mm fraction}}{\text{Total initial dry waste mass}}$$

63 1.

$$64 \quad \gamma_{B,I} \left( \frac{\text{kg}}{\text{m}^3} \right) = \frac{B_0(\%)}{100} \times \gamma_{d,I} \left( \frac{\text{kg}}{\text{m}^3} \right)$$

65 2.

66 where,  $B_0$  (dry mass/dry mass %) is the percentage of biodegradable waste prior to degradation  
67 and is defined as the proportion by dry mass of food, wood and paper plus the mass of VS in 20  
68 mm fraction of the entire dry waste mass (Fei and Zekkos, 2018).  $\gamma_{d,I}$  is the dry unit weight of  
69 the specimen after immediate compression was practically completed. The initial total mass,  
70 mass percentage, initial average moisture content, volatile solids (VS) in <20 mm fraction and  
71 initial density of biodegradable waste (Fei and Zekkos, 2018) are provided in Table 1. Briefly,  
72 AZ waste is “waste-rich” containing the highest amount of biodegradable material per unit  
73 volume ( $\gamma_{B,I} = 140 \text{ kg/m}^3$ ), while CA waste contains the least biodegradable material per unit  
74 volume ( $\gamma_{B,I} = 67 \text{ kg/m}^3$ ) and is “soil-rich”; TX waste is intermediately biodegradable ( $\gamma_{B,I} = 97$   
75  $\text{kg/m}^3$ ).

## 77 **2.2 Degradation testing of MSW**

78 The specimens were reconstituted based on their field waste composition and placed in 42-L  
79 columns for degradation testing. Three 42-L (d=300 mm, h=600 mm) columns accompanied by  
80 systems to recirculate and store leachate, and systems to monitor the long-term waste  
81 degradation process including biogas, changes in solid weight and volume were constructed as  
82 shown in Figure 1 and is described in detail by Fei et al. (2014). The materials were placed at a  
83 loose state, i.e., without significant compaction. Besides the vertical load from a plastic leachate  
84 distribution plate and a stainless steel rod for settlement measurement that impose <1 kPa  
85 vertical stress, no additional vertical stress was applied to the specimens. The temperature of  
86 each column remained constant at  $40 \pm 3^\circ\text{C}$  using a heating blanket. Leachate was recirculated  
87 three times a week and involved short-term (~15 min) submergence of the specimens followed

1 88 by gravity drainage of the liquids through the base of the column. Thus, the specimens were  
2 89 maintained at field capacity in between submergence events. Leachate samples were analysed  
3  
4 90 for pH and soluble chemical oxygen demand (APHA 2005). The concentrations of volatile fatty  
5  
6 91 acids (VFAs) in the samples were analysed using an ion chromatography system. The  
7  
8 92 specimen total weights at field capacity and when submerged were measured with time using  
9  
10 93 the weighing scales on which the setups were placed. Biogas composition was measured by a  
11  
12 94 gas chromatograph equipped with a thermal conductivity detector using nitrogen as the carrier  
13  
14 95 gas. The settlement in the specimen was measured continuously using a cable extension  
15  
16 96 transducer positioned above the column. The volume of generated biogas was measured by a  
17  
18 97 mass flow meter and was adjusted to standard temperature and pressure. The experiments  
19  
20 98 were considered complete after 885 days, 1500 days and 850 days of operation for AZ, TX and  
21  
22 99 CA specimens, respectively, since no additional biogas generation was observed, and further  
23  
24 100 settlement was considered minimal, and the setups were disassembled.

26 101

### 28 102 **3. Modelling Framework**

30 103

#### 32 104 ***3.1 HBM-Biodegradation Model***

34 105 The HBM biodegradation model (McDougall 2007) is incorporated in MATLAB, considering the  
35  
36 106 specimen column as a single element, with time as the evolving parameter. The model  
37  
38 107 describes a two-stage anaerobic digester in which volatile fatty acid (VFA) and methanogenic  
39  
40 108 biomass (MB) concentrations are the main field variables. Solid degradable fraction (SDF)  
41  
42 109 depletion is calculated for each time step and is controlled by the VFA and MB concentrations  
43  
44 110 and moisture content. The kinetics of the stoichiometry are controlled by growth and decay  
45  
46 111 parameters for each of the biodegradation variables,

- 48 112 •  $c$  [ $\text{g}\cdot\text{m}^{-3}$ ] the VFA concentration in aqueous medium;
- 50 113 •  $m$  [ $\text{g}\cdot\text{m}^{-3}$ ] the methanogen biomass (MB) in aqueous medium.

52 114 as set out in the following sections. In general, reaction rate equations are expressed in  
53  
54 115  $\text{g}\cdot\text{m}^{-3}\text{aqueous}\cdot\text{day}^{-1}$ .

56 116

1 117 Cellulose and hemicellulose are the major biodegradable components of MSW. However, in this  
2 118 model, mineralisation of only cellulose has been considered which accounts for 91% of the  
3  
4 119 methane potential for typical MSW (Barlaz et al., 1989). The process of cellulose degradation is  
5  
6 120 idealised in three main steps:  
7  
8 121 A. Enzymatic hydrolysis of solid cellulose ( $C_6H_{10}O_5$ ) to glucose ( $C_6H_{12}O_6$ ):  
9  
10 122  $C_6H_{10}O_5 + H_2O \rightarrow C_6H_{12}O_6$   
11  
12 123 B. Fermentation of glucose to acetic acid ( $CH_3COOH$ ) which is considered a representative  
13  
14 124 VFA:  
15  
16 125  $C_6H_{12}O_6 + 4H_2O \rightarrow CH_3COOH + 8H_2 + 4CO_2$   
17  
18 126 C. Methanogenesis:  
19  
20 127 (i) By acetate-cleaving methanogen:  
21  
22 128  $CH_3COOH \rightarrow CO_2 + CH_4$   
23  
24 129 (ii) By hydrogen-scavenging methanogen:  
25  
26 130  $4H_2 + CO_2 \rightarrow CH_4 + 2H_2O$   
27  
28 131  
29  
30 132 Assuming the fermentation process (acidogenesis and acetogenesis) is relatively fast compared  
31  
32 133 to methanogenesis and hydrogen-scavenging methanogens consume all gaseous intermediates  
33  
34 134 (step C (ii)), the overall stoichiometry is  
35  
36 135  $C_6H_{10}O_5 + H_2O \rightarrow CH_3COOH + 8H_2 + 4CO_2 \rightarrow 3CO_2 + 3CH_4$   
37  
38 136  
39  
40  
41 137 *3.1.1 Hydrolysis and acidogenesis/acetogenesis*  
42  
43 138 Hydrolysis and acidogenesis/acetogenesis is the first stage of the biodegradation, which  
44  
45 139 represents the depletion of the complex organic content and its transformation into VFA. These  
46  
47 140 latter intermediate products serve as a substrate for methanogenic biomass. However, high  
48  
49 141 VFA concentration has inhibitory effects on those reactions, which is also taken into account in  
50  
51 142 the model through an inhibitor factor.  
52  
53 143  
54  
55 144 An enzymatic hydrolysis function accounts for the influence of the changing digestibility of the  
56  
57 145 degradable fraction, product inhibition and moisture content on hydrolysis:



1 146  $r_g = \theta_E b \phi P$

2  
3 147 3.

4  
5 148 where,  $r_g$  denotes the rate of VFA accumulation [ $\text{g VFA} \cdot \text{m}^{-3} \text{ aqueous} \cdot \text{day}^{-1}$ ] and the four  
6  
7 149 governing factors are:

- 8  
9 150 •  $\theta_E$  is the effective volumetric moisture content which is determined from the hydraulic  
10  
11 151 model.  
12  
13 152 •  $b$  [ $\text{g} \cdot \text{m}^{-3} \text{ aqueous} \cdot \text{day}^{-1}$ ] is the maximum VFA growth rate under the most favourable  
14  
15 153 environmental conditions, which normally occurs at the early stage of hydrolysis  
16  
17 154 reaction.  
18  
19 155 •  $\phi = 1 - [(S_0 - S)/S_0]^n$  is the relative digestibility decreasing with the solid degradable  
20  
21 156 matter depletion, where  $S_0$  [ $\text{g} \cdot \text{m}^{-3}$ ] is the initial solid degradable fraction,  $S$  is the solid  
22  
23 157 degradable fraction at any time and  $n$  is the structural transformation parameter.  
24  
25 158 •  $P = \exp(-k_{VFA}(c))$  is the inhibition factor accounting for the inhibitory effect of high VFA  
26  
27 159 concentration, in which  $k_{VFA}$  [ $\text{g} \cdot \text{m}^{-3}$ ] is an inhibition constant.  
28  
29  
30 160

31 161 Note that in the modelling effort, because the specimen was completely submerged and then  
32  
33 162 drained to field capacity, the flow/hydraulics component of the model is not needed and the  
34  
35 163 effective volumetric moisture content ( $\theta_E$ ) is treated as the average field capacity moisture  
36  
37 164 content of the waste specimen after recirculation.  
38  
39

40 165

41  
42 166 *3.1.2 Methanogenesis*

43  
44 167 The second stage of the biochemical reactions occurring in the MSW transforms the VFA  
45  
46 168 generated in the first stage to methanogen biomass. The MB production rate  $r_j$  is calculated  
47  
48 169 through a Monod kinetic equation and the VFA consumption rate  $r_h$  is directly linked to the  
49  
50 170 methanogen biomass accumulation through a substrate yield coefficient  $Y$ .  
51

52  
53 171 
$$r_j = \frac{k_0 c}{(k_{MC} + c)} m$$

54  
55  
56 172 4.  
57  
58  
59  
60  
61  
62  
63  
64  
65

1  
2  
3  
4  
5  
6  
7  
8  
9  
10  
11  
12  
13  
14  
15  
16  
17  
18  
19  
20  
21  
22  
23  
24  
25  
26  
27  
28  
29  
30  
31  
32  
33  
34  
35  
36  
37  
38  
39  
40  
41  
42  
43  
44  
45  
46  
47  
48  
49  
50  
51  
52  
53  
54  
55  
56  
57  
58  
59  
60  
61  
62  
63  
64  
65

173  $r_h = \frac{r_j}{Y}$

174 5.

175 where  $k_0$  [day<sup>-1</sup>] is the maximum specific growth rate,  $k_{MC}$  [g.m<sup>-3</sup> aqueous] is the half saturation  
176 constant. The MB decay  $r_k$  is given by

177  $r_k = k_2 m$

178 6.

179 where,  $k_2$  [day<sup>-1</sup>] is the methanogen death rate.

180

181 *3.1.3 Governing Equations*

182 The combined growth and decay of VFA and MB in the biodegradation model are described by  
183 the following two equations:

184  $[r_g - r_h] = \frac{\partial c}{\partial t}$

185 7.

186  $[r_j - r_k] = \frac{\partial m}{\partial t}$

187 8.

188 The two simultaneous ordinary differential equations are solved iteratively by updating system  
189 parameters until a consistent solution is obtained which agrees well with the experimental data.

190 The solid degradable fraction is depleted in each timestep using the following equation

191  $S^{t+\Delta t} = S^t - \theta \cdot \frac{162}{60} r_g \Delta t$

192 9.

193 where,  $S^t$  is the solid degradable fraction remaining in timestep  $t$  and  $t + \Delta t$  is the next time step.

194 This is derived from the overall stoichiometry which indicates 60 g of acetic acid (representative  
195 VFA) is a result of the solubilisation of 162 g of cellulose. The stoichiometry of the hydrolytic  
196 step shows that 162 g of cellulose consumes 18 g of water; hence the effective volumetric  
197 moisture content is also decreased in each timestep by

1 198  $d\theta = \frac{18}{162\rho_{H_2O}} dS$

4 199 10.

6 200 where,  $\rho_{H_2O}$  is the density of water.

9 201

11 202 *3.1.4 Methane Generation*

13 203 In the HBM model, methane production (and carbon dioxide) is estimated from the stoichiometry  
 14 204 of the digestion process. In other words, assuming the solid degradable fraction to consist  
 15 205 purely of cellulose, then 1 mole of cellulose gives rise to 3 moles of carbon dioxide and 3 moles  
 16 206 of methane.

21 207

23 208 *3.1.5 Biodegradation-induced settlement*

25 209 A constitutive relationship between decomposition of solid degradable fraction, i.e. a change in  
 26 210 solid phase volume  $V_S$ , and the induced change in void volume  $V_V$  (McDougall and Pyrah 2004),  
 27 211 is implemented to calculate the change in void ratio in the MSW matrix and subsequently, the  
 28 212 strain due to biodegradation  $\varepsilon_B$  is calculated.

33 213  $dV_V = \Lambda dV_S$

35 214 11.

38 215  $de = (e - \Lambda) \frac{dV_S}{V_S}$

41 216 12.

45 217  $\varepsilon_B = \frac{de}{1 + e_0}$

48 218 13.

50 219 where,  $\Lambda$  is the decomposition (or degradation)-induced void change parameter,  $e$  is the void  
 51 220 ratio and  $e_0$  is the initial void ratio.

54 221

56 222 *3.1.6 Settlement due to time-dependent creep*

223 Creep behaviour is incorporated within the HBM model using the 'equivalent time' method (Yin  
224 and Graham, 1989). 'Equivalent time' allows the creep strain rate of an over-consolidated  
225 material and its hardening to be related to the normal consolidation line at all stages of loading.

226 Creep strains at constant effective stress for incremental loading are modelled by

$$227 \frac{de}{dt} = \left( \frac{\chi}{t + t_0 + t_{eq} + t_{ref}} \right)$$

228 14.

229 where,  $e$  is the void ratio,  $t$  is the current time,  $t_0$  is the time at which the current creep stage  
230 commences  $t_{eq}$  is the equivalent time,  $t_{ref}$  is the reference time to indicate when creep straining  
231 commences (a curve fitting parameter unique to each specimen) and  $\chi$  is the creep viscosity  
232 coefficient.  $\chi$  is a material parameter and constant for a given waste specimen. In this study, it is  
233 considered that the equivalent time is close to the duration of the increments since the  
234 specimen is in normally consolidated range of loading (Yin and Graham, 1994).

235

### 236 **3.2 Initial Conditions**

237 The solid fraction is segregated into degradable and inert phases for input into the HBM model.

238 Initial solid degradable fraction ( $S_0$ ) and degradable phase density are determined from the  
239 waste composition as provided in Table 2. Determination of each phase density requires the  
240 density of each solid constituent in the waste (paper, wood, plastic and <20 mm fraction).

241 Particles <20 mm (soil-like fraction) consist of inorganic soil intermixed with degradable and  
242 inert particles. The organic content (in terms of volatile solids) in that fraction varies from 7% to  
243 13% in the three specimens. Since, the specific gravity ( $G_s$ ) of soil decreases with increasing  
244 organic content (Radforth et al., 1996), the soil-like fraction  $G_s$  varies from 2.0 to 2.4 (solid  
245 phase density of 2000 kg/m<sup>3</sup> to 2400 kg/m<sup>3</sup>). Nevertheless, it is observed that the modelling  
246 results are not affected significantly by different  $G_s$  for the range of waste composition  
247 considered. Based on this calculation, 24%, 12% and 9% by dry weight of the MSW solids are  
248 degradable in AZ, TX and CA specimens, respectively, as shown in Table 3.

249

### 250 **3.3 Modelling Strategy**

1 251 As-placed physical waste characteristics, i.e., initial mass, height and volume, are defined.  
2 252 Initially a simulation was run adopting the default parameters as provided in McDougall (2007).  
3  
4 253 However, the results fit the experimental data poorly which is not surprising. As a result, all the  
5  
6 254 biodegradation parameters were adjusted to improve the fit between the HBM model and  
7  
8 255 experimental data. The parameter values that most closely match the experimental data for the  
9  
10 256 selected MSW specimens are provided in Table 4.

11  
12 257

## 13 14 258 **4. Results**

### 15 16 259 **4.1 VFA and MB concentrations**

17  
18 260 Figure 2 shows the evolution of VFA as a function of time for all specimens. A good fit is  
19  
20 261 observed between the experimental data and the model prediction of the VFA concentrations.  
21  
22 262 Initial VFA and MB concentrations are chosen as shown in Table 4 to best match the  
23  
24 263 experimental data. The VFA concentration starts from an initial value, reaches a peak and  
25  
26 264 decays soon reaching a long-term residual value indicative of established methanogenesis. It is  
27  
28 265 interesting to note that initial VFA for “waste-rich” AZ specimen is high (8500 g/m<sup>3</sup>) indicating  
29  
30 266 that anaerobic process readily established in the waste mass. The AZ specimen produced the  
31  
32 267 highest VFA (peaks at 13500 g/m<sup>3</sup>) indicating more biodegradable material available for  
33  
34 268 hydrolysis and fermentation to take place, followed by the intermediate biodegradable TX  
35  
36 269 specimen (peaks at 4750 g/m<sup>3</sup>) and then the “soil-rich” least biodegradable CA specimen  
37  
38 270 (peaks at 450 g/m<sup>3</sup>). The model predicts lower decay rates of VFA than the measured data in  
39  
40 271 TX and CA specimens. For example, the measured VFA concentration in TX specimen reduces  
41  
42 272 to a value close to zero at day 50, whereas the model reaches zero at around day 90. The  
43  
44 273 maximum VFA concentrations are constrained by the product inhibition factor, whereas their  
45  
46 274 subsequent decay is triggered by MB accumulation. The residual input parameters were  
47  
48 275 therefore tuned by a combination of an increase in maximum hydrolysis rate (to stimulate initial  
49  
50 276 VFA accumulation), a reduction in the product inhibition factor (to allow higher peak VFA  
51  
52 277 concentration) and an increase in methanogen growth rate (to accelerate MB accumulation and  
53  
54 278 thereby accelerate post-peak decay in VFA concentrations). Peak VFA concentrations  
55  
56 279 increases with increase in maximum hydrolysis rates and decreases with increase in product  
57  
58 280 inhibition factor (Table 4). As the waste becomes more degradable, maximum VFA  
59  
60  
61  
62  
63  
64  
65

1 281 concentrations occur later. For example, AZ peaks after around 25 days while CA peaks after 5  
2 282 days.

3  
4 283

5  
6 284 Figure 3 shows methanogenic biomass accumulation predicted by HBM. Initial MB  
7  
8 285 concentration ranges from 1200 g/m<sup>3</sup> for “waste-rich” AZ specimen to 10 g/m<sup>3</sup> for “soil-rich” CA  
9  
10 286 specimen as shown in Table 4. Initial MB concentration influences VFA accumulation and  
11  
12 287 through product inhibition controls hydrolysis, subsequent MB growth and the onset of  
13  
14 288 methanogenesis (McDougall and Philp, 2001). It is evident that the more-biodegradable AZ  
15  
16 289 specimen produces the maximum MB accumulation (peaks at 19000 mg/L) and CA produces  
17  
18 290 the minimum (peaks at 4700 mg/L), with TX reaching an intermediate value (peaks at 8200  
19  
20 291 mg/L). However, it is interesting to note that, with the increase in biodegradability, the MB peaks  
21  
22 292 are slightly delayed with AZ reaching the maximum in 85 days while TX and CA attaining its  
23  
24 293 peak in 75 days. The methanogen yield coefficient ( $Y$ ) controls the mass of methanogenic  
25  
26 294 biomass produced per unit mass of substrate with AZ and TX having higher values than CA  
27  
28 295 (Table 4). As the biodegradability of waste increases, an increase in half-saturation constant  
29  
30 296 and methanogen death rate and a decrease in specific growth rate of cellulose is observed  
31  
32 297 (Table 4). Note that MB concentrations were not measured during the experiment (Fei et al.,  
33  
34 298 2015).

35  
36  
37 299

#### 38 39 300 **4.2 Solid degradable fraction**

40  
41 301 Figure 4 shows that the stock of solid degradable fraction or organic fraction was almost  
42  
43 302 completely mineralised during the course of the experiment (in 300 days) and all metabolic  
44  
45 303 processes slowed down as a result. The solid degradable fraction depletion predicted by HBM  
46  
47 304 fit fairly well with the experimental data except for the initial 20-30 days. The initial “rise” in the  
48  
49 305 experimental data during the first 20-30 days is due to the initial adjustment of the solid  
50  
51 306 components in the loose waste matrix and changes in the volume during the first 1-3 leachate  
52  
53 307 recirculation events, after which the biodegradation process begins. It is evident that “waste-  
54  
55 308 rich” AZ specimen has the maximum initial stock of organic fraction (102 kg/m<sup>3</sup>), while “soil-rich”  
56  
57 309 CA specimen has the minimum value (50 kg/m<sup>3</sup>). Also, with increase in biodegradability in  
58  
59 310 waste, the solids depletion rate increases. AZ solids deplete faster than TX and CA solids. It is

1 311 observed that MB growth depends on the amount of solid degradable fraction remaining. With  
2 312 the complete depletion of solids at around 300 days, the MB concentrations also decay to  
3  
4 313 negligible values. Note that during the experiments there was no direct measurement of solids  
5  
6 314 depletion. However, it is calculated indirectly by considering the consumption of degradable  
7  
8 315 solids being proportional to the measured biogas production which is a reasonable assumption  
9  
10 316 considering the stoichiometry of the anaerobic process. It is interesting to note that the reduction  
11  
12 317 of moisture at the end of degradation (Equation 10) is approximately 3.2% for AZ, 1.6% for TX  
13  
14 318 and 1.4% for CA, which is not considered significant.  
15

16 319

### 18 320 **4.3 Methane generation**

20 321 Figure 5 shows the cumulative methane generation for the specimen. As waste becomes more  
21  
22 322 degradable, methane generation increases. It is observed that the total volume of methane  
23  
24 323 collected during the experiment is 1110 L for AZ, 476 L for TX and 187 L for CA (methane:  
25  
26 324 carbon dioxide measured approximately equal to 60:40) while the model predicts a total of 1681  
27  
28 325 L for AZ, 1110 L for TX and 879 L for CA (methane: carbon dioxide equal to 50:50). Clearly,  
29  
30 326 methane production is over-predicted by the model – more for the “soil rich” specimen than  
31  
32 327 “waste rich”, possibly due to the simplified stoichiometric assumption of solid degradable  
33  
34 328 fraction of MSW consisting of only cellulose. Apart from cellulose, hemicellulose is another  
35  
36 329 principal biodegradable component of MSW; while the other major organic component, lignin, is  
37  
38 330 at best only slowly degradable under methanogenic conditions and acts as a recalcitrant.  
39  
40 331 (Barlaz et al., 1990). In addition, the experimental methane yield could be lower due to a  
41  
42 332 number of factors such as part of the organic material inaccessible due to binding in particles or  
43  
44 333 structural organic matter, utilization of a fraction of the substrate to synthesize bacterial mass,  
45  
46 334 ammonia toxicity or limitation of other nutrient factors (Angelidaki et al., 2004, Labatut et al.,  
47  
48 335 2010).

50 336

### 53 337 **4.4 Settlement**

55 338 Figure 6 shows the model prediction of the evolution of the biodegradation and creep strain  
56  
57 339 (settlement) along with the experiment settlement data. Long-term settlement of waste  
58  
59 340 specimen is found to follow three phases – immediate compression, active biodegradation and

1 341 residual compression, as discussed in Fei and Zekkos (2013). Immediate compression occurs  
2 342 as a result of loose placement of the waste material in the column and due to changes in  
3  
4 343 volume owing to softening associated with moistening, waste structure adjustment and particle  
5  
6 344 movement, particularly during the first few recirculation events. Active biodegradation occurs  
7  
8 345 when most microbial species reach their maximum growth rates, and a robust microbial  
9  
10 346 community has been established. Residual compression occurs when settlement slows down  
11  
12 347 due to retarded microbial activity and creep becomes a major contributor to the settlement (Fei  
13  
14 348 and Zekkos, 2013). For a typical waste composition as in AZ, immediate compression of the  
15  
16 349 waste mass was observed between days 1-10. Active biodegradation took place from day 10 to  
17  
18 350 day 270 and the remaining was residual compression.  
19

20 351

21  
22 352 In this study, only active biodegradation strain and residual compression (in terms of creep  
23  
24 353 strain) has been modelled. Biodegradation induced strain, as predicted by the model, is a  
25  
26 354 function of the volume of solids and the void ratio. The trend of the model is generally consistent  
27  
28 355 with the experimental data. AZ (“waste-rich”) has attained the maximum settlement (in terms of  
29  
30 356 strain) while CA (“soil-rich”) attained the minimum settlement. The model predictions for the  
31  
32 357 final settlement (except immediate compression) are close to the experimental values. For  
33  
34 358 example, for AZ, the final strain in the experimental setup was recorded as 32%, while the  
35  
36 359 model predicts a strain of 28.5%. Immediate compression occurs in the specimens during the  
37  
38 360 first 1-3 leachate recirculation events (till 5-10 days), which is not modelled in this study as  
39  
40 361 shown in Figure 6. AZ and CA specimens have significant immediate strains of 10.9% and 10%,  
41  
42 362 respectively, while TX has a noticeably low value of 1.5%.  
43  
44

45 363

46  
47 364 The decomposition-induced void change parameter ( $\lambda$ ) is an effective constitutive link between  
48  
49 365 the mechanical consequences of decomposition and their biochemical causes (McDougall and  
50  
51 366 Pyrah, 2004).  $\lambda$  values are obtained in this study (Table 4) by approximately matching the slope  
52  
53 367 of the biodegradation-induced settlement curve of the experiment with the model. Values are  
54  
55 368 similar for all three specimens (0.8 for AZ, 0.7 for TX and 0.8 for CA) and are estimated to be  
56  
57 369 less than the specimen void ratio at any time ( $e$  estimated to be between 1.7 and 2.4 for AZ, 1.4  
58  
59 370 and 1.7 for TX, 1.7 and 1.8 for CA), which indicates loosening and possible weakening of the  
60  
61  
62  
63  
64  
65



1 371 material after degradation. Although the parameter values are not found to change significantly  
2 372 with waste composition in this study, factors such as compaction effort and vertical stress that  
3  
4 373 were not investigated in this study, may influence them. In addition, a systematic trend in creep  
5  
6 374 viscosity coefficient ( $\chi$ ) in the three specimens (Table 4) is observed with AZ having the highest  
7  
8 375 value of 0.018 and CA the lowest value of 0.007. This is indicative of the fact that waste  
9  
10 376 constituents have an impact on the time-dependent creep of a soil-waste mixture (Zekkos et al.,  
11  
12 377 2016). For example, AZ has the maximum amount of paper and soft plastic than the other two  
13  
14 378 specimens which results in significant creep in the specimen. Note that in this study, both the  
15  
16 379 experiment and the model consider negligible vertical stress on the specimen.  
17

18 380

## 20 381 **5. Conclusion**

22 382 The coupled biochemical-physical-mechanical processes documented during the degradation of  
23  
24 383 MSW in a large-scale experimental setup is modelled using the HBM-biodegradation  
25  
26 384 framework. The VFA and MB concentrations (biochemical) are dependent on the solid  
27  
28 385 degradable fraction (physical), which is in turn coupled with biodegradation-induced vertical  
29  
30 386 strain. For a given waste composition, the model parameters are calibrated against the  
31  
32 387 experimental data. Influence of waste composition on this coupled behaviour has been  
33  
34 388 investigated through three significantly different MSW specimens. The most significant findings  
35  
36 389 from this work are as follows:

- 37 390 • The model predicts aspects of biochemical and physical behaviour fairly well.
- 38 391 • Biodegradation and creep induced settlement trends (mechanical behaviour) agree well  
39 392 with the experimental results.
- 40 393 • Specific gravity of soil-like (<20 mm) fraction (varying from 2.0-2.4) does not have significant  
41 394 effect on the degradation process.
- 42 395 • Decomposition-induced void-change parameter values do not change significantly with  
43 396 waste composition.
- 44 397 • With increase in biodegradability of waste, an increase in VFA and MB accumulation,  
45 398 increase in depletion rate of organic fraction, increase in methane production, and increase  
46 399 in settlement are observed.

1 400 • The model systematically over predicts methane production; more so for the “soil-rich”  
2 401 specimen than the “waste-rich”.  
3  
4 402 Note that the model formulation considered here is one-dimensional and time is the only varying  
5  
6 403 parameter. This is adequate for the purposes of modelling these specific laboratory  
7  
8 404 experiments. However, MSW in the field is essentially heterogeneous and anisotropic, hence, it  
9  
10 405 becomes critical that spatial variability is considered as well. In addition, in this study, both  
11  
12 406 experimentally and numerically, the degradation process was conducted under negligible  
13  
14 407 vertical stress.  
15

16 408

### 18 409 **Acknowledgements**

20 410 This research was supported by the National Science Foundation (NSF) Division of Computer  
21  
22 411 and Communication Foundations under Grant no. 1442773 and Environmental Research and  
23  
24 412 Education Foundation (EREF) Scholarship. ConeTec Investigations Ltd. and the ConeTec  
25  
26 413 Education Foundation are acknowledged for their support to the Geotechnical Engineering  
27  
28 414 Laboratories at the University of Michigan. Any opinions, findings, conclusions and  
29  
30 415 recommendations expressed in this paper are those of the authors and do not necessarily  
31  
32 416 reflect the views of the NSF, EREF or ConeTec.  
33

34 417

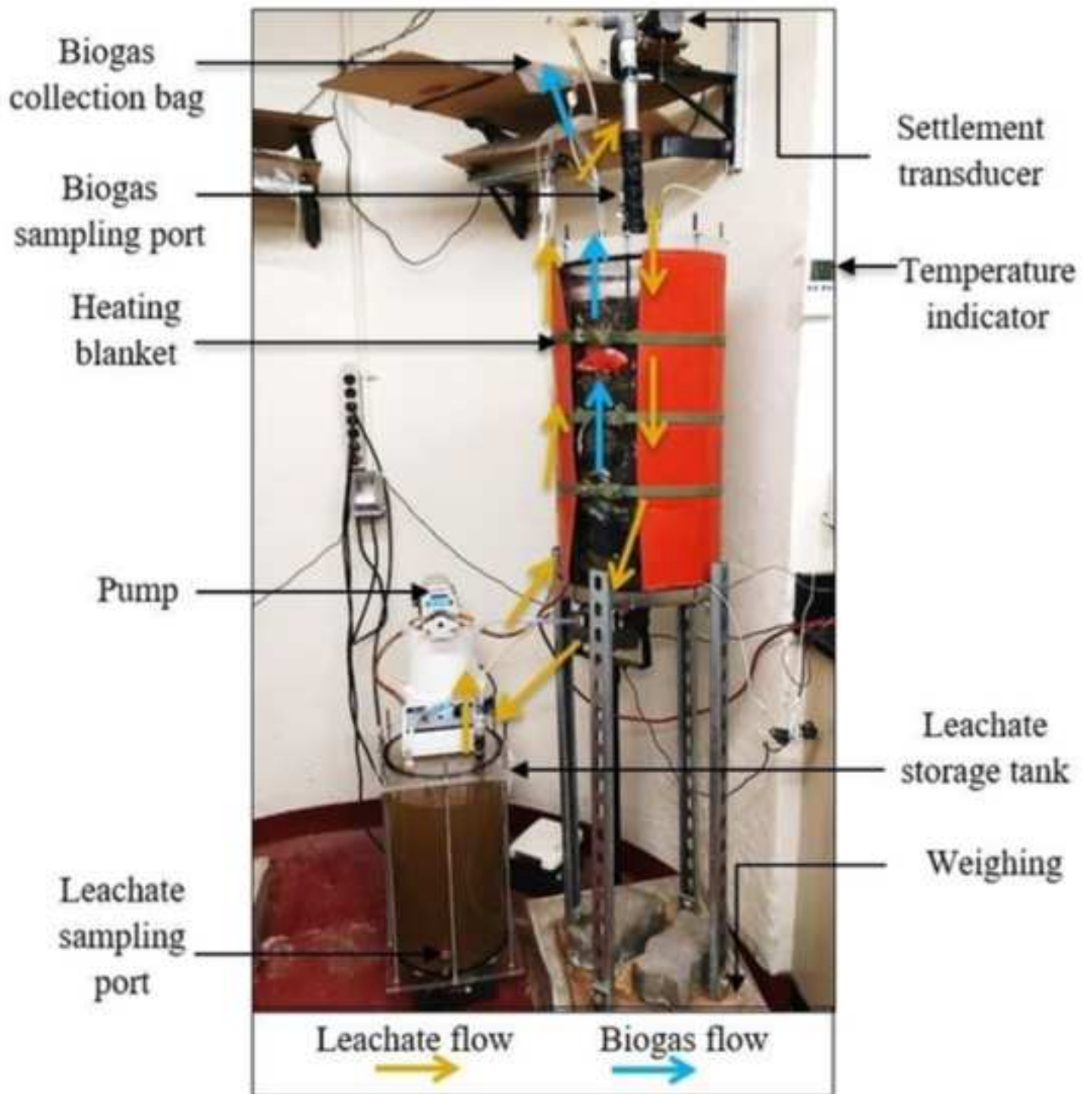
### 36 418 **References**

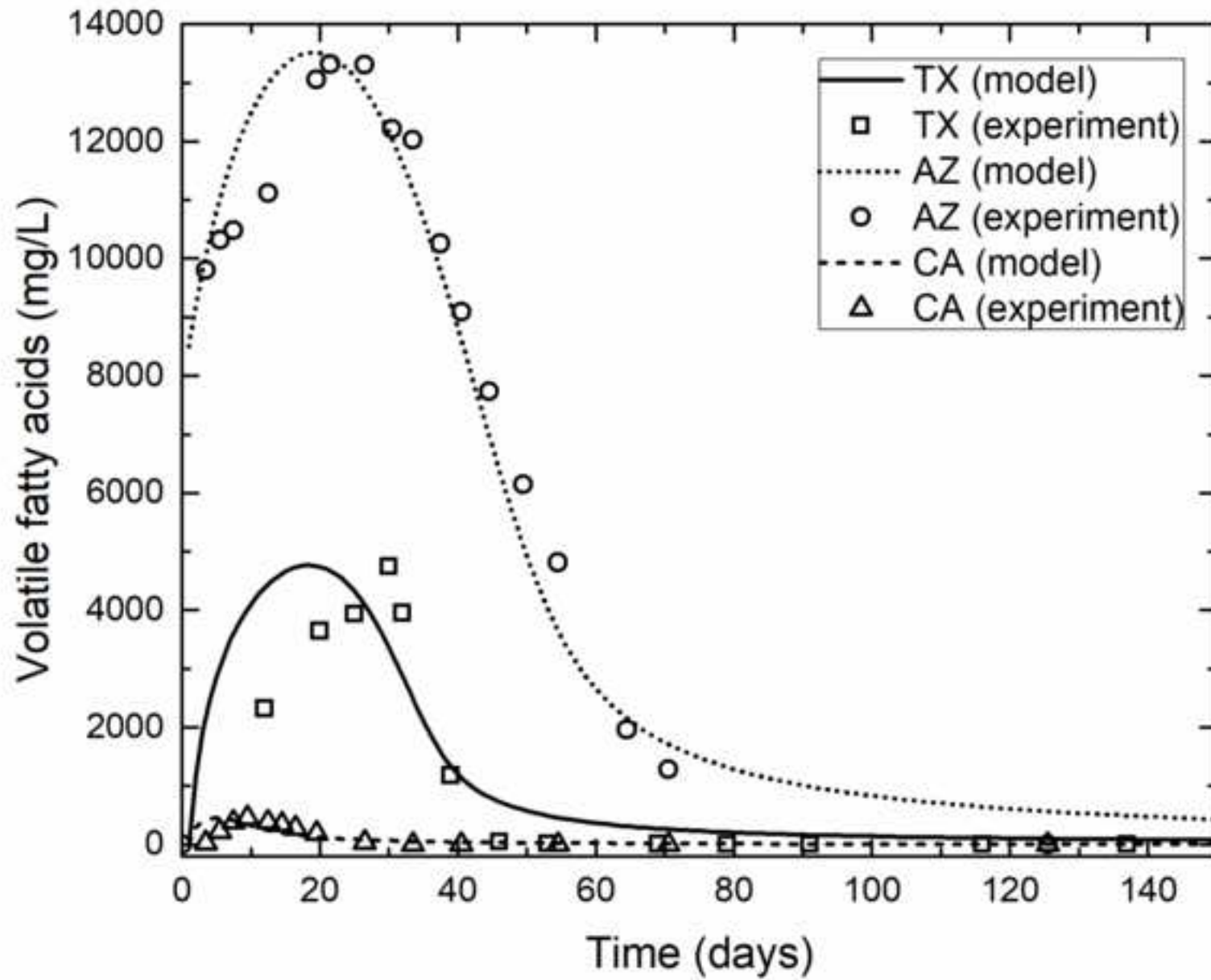
38 419 APHA (2005) Standard Methods for the Examination of Water and Wastewater, American  
39  
40 420 Public Health Association, Washington, D.C  
41  
42 421 Angelidaki I and Sanders W (2004) Assessment of The Anaerobic Biodegradability Of  
43  
44 422 Macropollutants, Rev Environ Sci Biotechnol, **3 (2)**, 117-129.  
45  
46 423 Barlaz MA, Ham RK and Schaefer DM (1989) Mass balance analysis of anaerobically  
47  
48 424 decomposed refuse. ASCE, J Env Eng Div, **115(6)**, 1088–102.  
49  
50 425 Barlaz MA, Ham RK, Schaefer DM and Isaacson R (1990) Methane production from municipal  
51  
52 426 refuse: a review of enhancement techniques and microbial dynamics. Critical Reviews in  
53  
54 427 Environmental Science and Technology, **19(6)**, 557-584.  
55  
56 428 Barlaz MA, Staley BF, and de los Reyes FL (2010) Anaerobic biodegradation of solid waste.  
57  
58 429 Environ. Microbiol., R Mitchell and J Gu (eds), Wiley-Blackwell, Hoboken, NJ, pp. 281-299.  
59  
60  
61  
62  
63  
64  
65

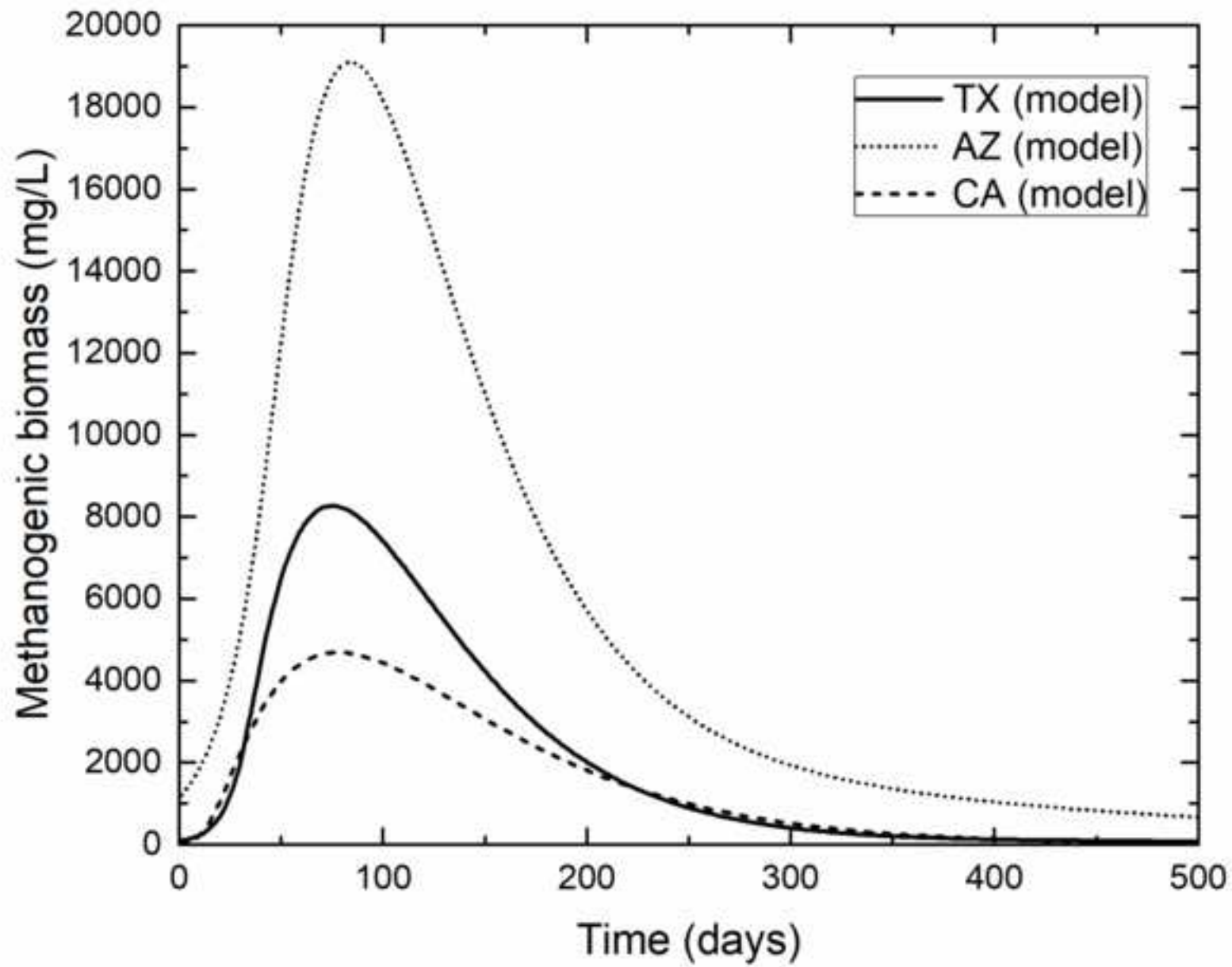
1 430 Batstone DJ, Keller J, Angelidaki I, Kalyuzhnyi SV, Pavlostathis SG, Rozzi A, Sanders WT,  
2 431 Siegrist H and Vavilin VA (2002). The IWA Anaerobic Digestion Model No 1 (ADM1). Water Sci  
3  
4 432 Technol., **45(10)**, 65-73.  
5  
6 433 Chakma S, Vaishya RC and Yadav AK (2016) Modeling chemical compositions of municipal  
7  
8 434 solid waste. Environmental Geotechnics, **3(2)**, 65-77.  
9  
10 435 Datta S, Zekkos D, Fei X and McDougall J (2017) Experimental Assessment and Modelling of  
11  
12 436 Coupled Biochemical-Physical-Mechanical Biodegradation Process of a Municipal Solid Waste  
13  
14 437 Sample from Michigan. In *Proceedings of the 2nd Symposium on Coupled Phenomena in*  
15  
16 438 *Environmental Geotechnics (CPEG2)*, Leeds, UK.  
17  
18 439 EPA (U.S. Environmental Protection Agency) (2014) Advancing Sustainable Materials  
19  
20 440 Management: Facts and Figures Fact Sheet, Office of Land and Emergency Management,  
21  
22 441 Washington DC, USA.  
23  
24 442 Fei X and Zekkos D (2013) Factors Influencing Long-Term Settlement of Municipal Solid Waste  
25  
26 443 in Laboratory Bioreactor Landfill Simulators. Journal of Hazardous, Toxic, and Radioactive  
27  
28 444 Waste, **17(4)**, 25-271.  
29  
30 445 Fei X, Zekkos D and Raskin L (2014) An Experimental Setup for Simultaneous Physical,  
31  
32 446 Geotechnical, and Biochemical Characterization of Municipal Solid Waste Undergoing  
33  
34 447 Biodegradation in the Laboratory. Geotechnical Testing Journal, 01/2014; **37(1)**:1-12. DOI:  
35  
36 448 10.1520/GTJ20130084.  
37  
38 449 Fei X and Zekkos D, and Raskin L (2015) Archaeal community structure in leachate and  
39  
40 450 municipal solid waste is correlated to the methane generation and volume reduction during  
41  
42 451 biodegradation of municipal solid waste. Waste Management, **36**, 184-190.  
43  
44 452 Fei X (2016) Experimental Assessment of Coupled Physical-Biochemical-Mechanical-Hydraulic  
45  
46 453 Processes of Municipal Solid Waste Undergoing Biodegradation. Ph.D. thesis, Department of  
47  
48 454 Civil and Environmental Engineering, University of Michigan, Ann Arbor.  
49  
50 455 Fei X and Zekkos D (2018) Coupled experimental assessment of physico-biochemical  
51  
52 456 characteristics of municipal solid waste undergoing enhanced biodegradation. Geotechnique,  
53  
54 457 DOI10.1680/jgeot.16.p.253.  
55  
56  
57  
58  
59  
60  
61  
62  
63  
64  
65

1 458 Gawande NA, Reinhart DR, and Yeh GT (2010) Modelling microbiological and chemical  
2 459 processes in municipal solid waste bioreactor, part i: development of a three-phase numerical  
3  
4 460 model biokemod-3p. *Waste Management*, **30(2)**, 202-210.  
5  
6 461 Labatut RA, Angenent LT and Scott NR (2011) Biochemical methane potential and  
7  
8 462 biodegradability of complex organic substrates. *Bioresource Technology*, **102**, 2255–2264.  
9  
10 463 Machado S, Vilar OM, Carvalho MF (2008) Constitutive model for long term municipal solid  
11  
12 464 waste mechanical behaviour. *Computers and Geotechnics*, **35(5)**, 775-790.  
13  
14 465 McDougall JR and Philp JC (2001) Parametric study of landfill biodegradation modelling:  
15  
16 466 methanogenesis & initial conditions. *In Proc. Sardinia 2001, 8th Intl. Waste Man. & Landfill*  
17  
18 467 *Symp.* Eds. Christensen TH, Cossu R & Stegmann R, CISA, Cagliari, Vol. 1, pp 79-88.  
19  
20 468 McDougall JR and Pyrah IC (2004) Phase relations for decomposable soils. *Geotechnique*,  
21  
22 469 **54(7)**, 487–94.  
23  
24 470 McDougall J (2007) A hydro-bio-mechanical model for settlement and other behaviour in  
25  
26 471 landfilled waste. *Comput. Geotech.*, **34(4)**, 229-246.  
27  
28 472 Milke M, Fang Y and John S (2010) Anaerobic biodegradability of wood: a preliminary review. In  
29  
30 473 *Engineering: Conference Contributions*. Civil and Natural Resources Engineering, University of  
31  
32 474 Canterbury, Christchurch, New Zealand.  
33  
34 475 Olivier F and Gourc JP (2006) Hydromechanical behaviour of municipal solid waste subject to  
35  
36 476 leachate recirculation in a large-scale compression reactor cell. *Waste Management*, **27(1)**, 44–  
37  
38 477 58.  
39  
40 478 Radforth NM and Brawner CO (1996) *Muskeg and the Northern Environment in Canada*,  
41  
42 479 University of Toronto Press, Toronto, Ontario, Canada.  
43  
44 480 Zekkos D, Bray JD, Kavazanjian E Jr et al. (2006) Unit weight of municipal solid waste. *Journal*  
45  
46 481 *of Geotechnical and Geoenvironmental Engineering*, **132(10)**, 1250-1261.  
47  
48 482 Zekkos D, Kavazanjian E, Bray JD, Matasovic N and Riemer MF (2010) Physical  
49  
50 483 Characterization of Municipal Solid Waste for Geotechnical Purposes. *Journal of Geotechnical*  
51  
52 484 *and Geoenvironmental Engineering*, **136(9)**, 1231-1241.  
53  
54 485 Zekkos D, Fei X, Grizi A, and Athanasopoulos G (2016) Response of municipal solid  
55  
56 486 waste to mechanical compression. *Journal of Geotechnical and Geoenvironmental*  
57  
58 487 *Engineering*, **143(3)**: 04016101  
59  
60  
61  
62  
63  
64  
65

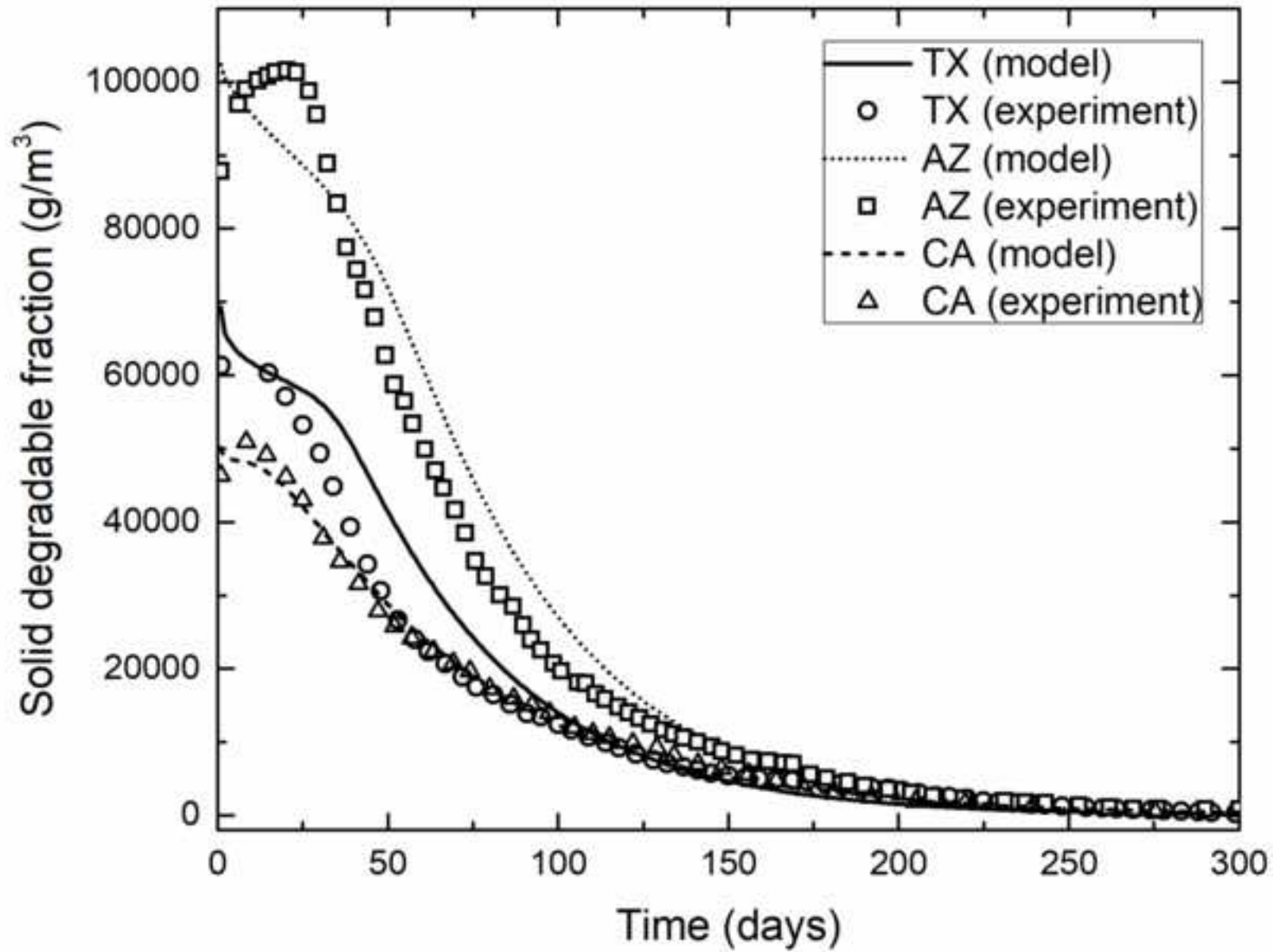
1 488 Zobel BL, and van Buijtenen JP (1989) Wood Variation: Its Causes and Control. In *Wood*  
2 489 *Variation and Properties*. Springer-Verlag, Berlin Heidelberg, pp. 1-32.  
3  
4 490  
5  
6 491 **Figure captions**  
7  
8 492 Figure 1. Schematic of the experimental setup (Datta et al., 2017)  
9  
10 493 Figure 2. VFA concentrations measured experimentally and predicted by HBM-biodegradation  
11  
12 494 model  
13  
14 495 Figure 3. Methanogenic biomass concentrations predicted by HBM-biodegradation model  
15  
16 496 Figure 4. Solid degradable fraction measured experimentally and predicted by HBM-  
17  
18 497 biodegradation model  
19  
20 498 Figure 5. Cumulative methane generation measured experimentally and predicted by HBM-  
21  
22 499 biodegradation model  
23  
24 500 Figure 6. Settlement (strains) measured experimentally and predicted by HBM-biodegradation  
25  
26 501 model (\*Immediate compression observed during the experiment, not modelled in this study)  
27  
28 502  
29  
30 503  
31  
32 504 **Table captions**  
33  
34 505 Table 1. Composition, moisture content, volatile solids and biodegradability of three MSW  
35  
36 506 specimens.  
37  
38 507 Table 2. Example calculation of solid degradable fraction from initial waste composition of TX  
39  
40 508 specimen.  
41  
42 509 Table 3. Initial modelling conditions for the three MSW specimens.  
43  
44 510 Table 4. HBM-Biodegradation calibrated model parameters for the three MSW specimens.  
45  
46  
47  
48  
49  
50  
51  
52  
53  
54  
55  
56  
57  
58  
59  
60  
61  
62  
63  
64  
65

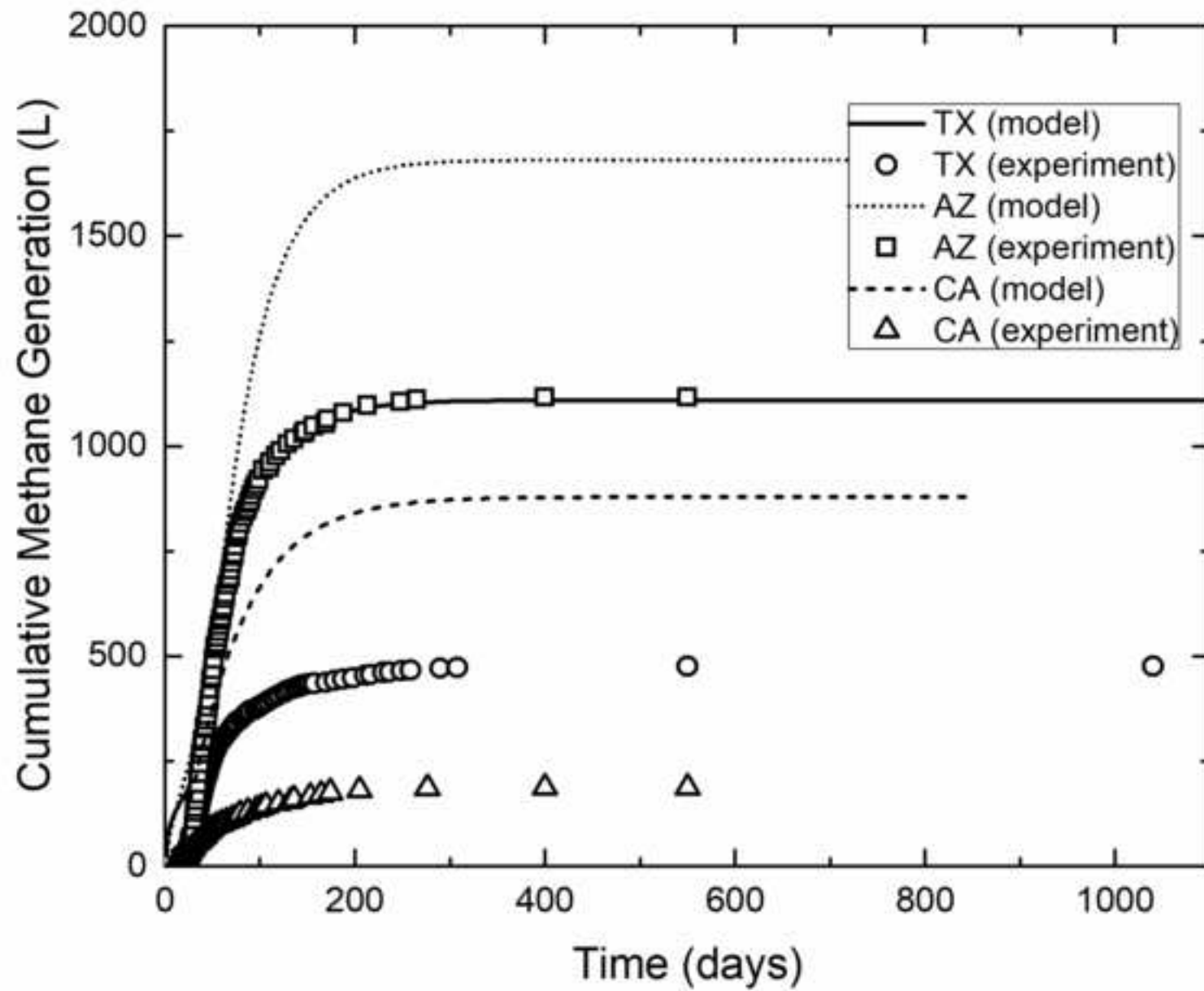












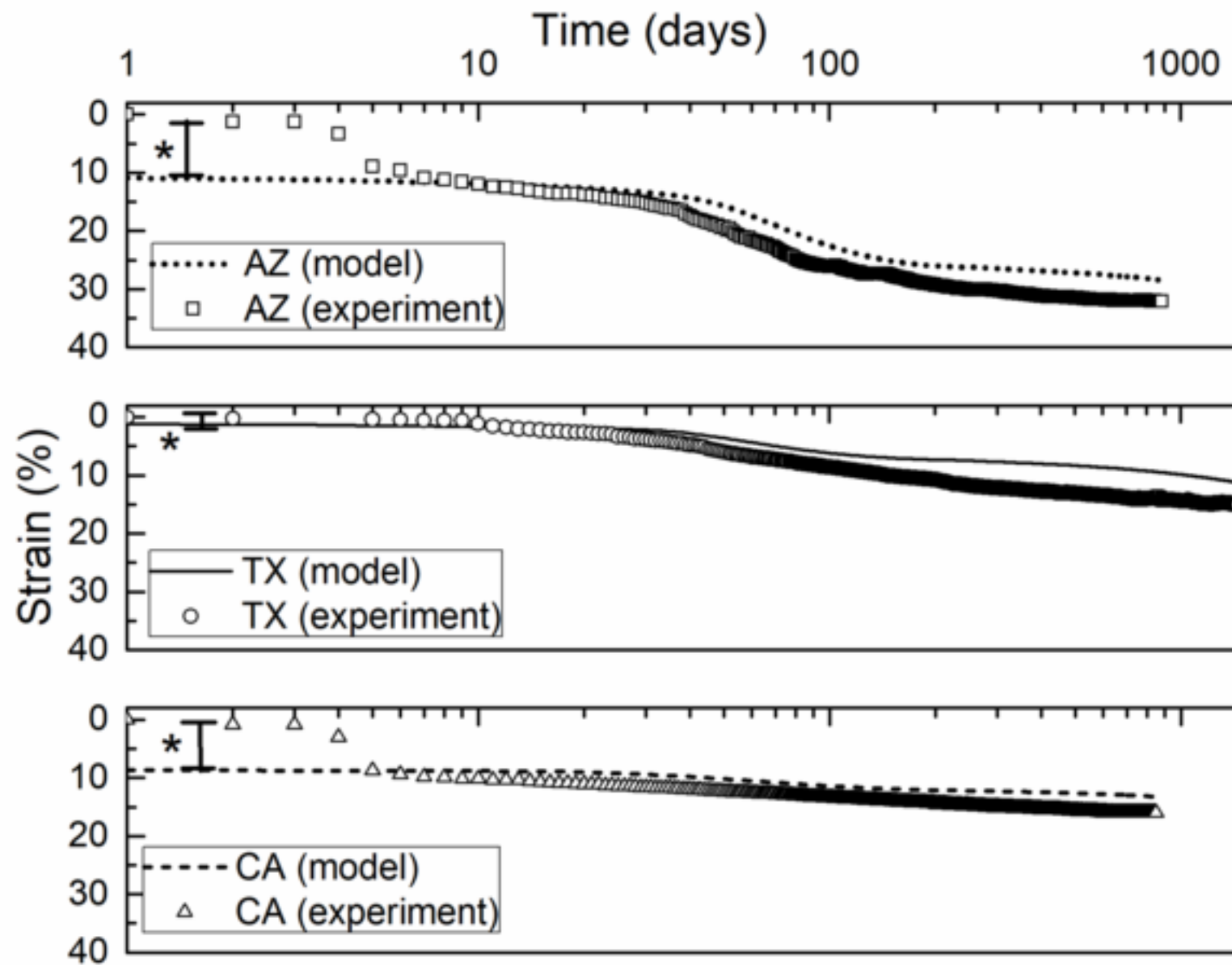


Table 1. Composition, moisture content, volatile solids and biodegradability of three MSW specimens.

Parameter	Value		
	AZ	TX	CA
Paper (%)	21.4	10.7	4.6
Wood (%)	2.1	4.3	5.8
Soft plastic (%)	8.5	5.9	3.9
<20 mm particles (%)	68.0	79.1	68.5
Hard plastic, metal, cobbles (%)	0	0	17.2
Initial total weight (kg)	21.69	29.31	29.02
Initial average moisture content (%)	32.7	37.7	28.1
Volatile solids in <20 mm fraction (g/g dry)	0.128	0.252	0.086
Initial percentage of biodegradable waste, $B_0$ (% dry)	30.1	16.2	10.5
Initial density of biodegradable waste, $\gamma_{B,I}$ (kg/m <sup>3</sup> )	140	97	67

Table 2. Example calculation of solid degradable fraction from initial waste composition of TX specimen.

Waste constituent	Dry weight (kg)	Degradable solids (kg dry)	Inert solids (kg dry)	Density of solid constituent (kg/m <sup>3</sup> )	Degradable phase density, $\rho_{sd}$ (kg dry/m <sup>3</sup> )	Inert phase density, $\rho_{si}$ (kg dry/m <sup>3</sup> )
Paper	2.3	1.5 <sup>a</sup>	0.8	810 <sup>b</sup>	1044 <sup>g</sup>	1727 <sup>g</sup>
Wood	0.9	0.1 <sup>d</sup>	0.8	600 <sup>e</sup>		
Soft Plastic	1.3	0	1.3	970 <sup>b</sup>		
<20 mm	16.9	0.9 <sup>f</sup>	15.9	2200 <sup>c</sup>		
Total (% dry weight)		11.7	88.3			

<sup>a</sup>Degradable fraction in paper waste is considered to be 20-80 % (Barlaz et al. 1990). For TX specimen, it is 65 %

<sup>b</sup>Olivier and Gourc, 2006

<sup>c</sup>Specific gravity of soil-like fraction with organic content considered to be the average of the range 2.0-2.4. (Radforth et al., 1996)

<sup>d</sup>Degradable fraction in wood is considered to be 0-20 % (Milke et al., 2010). For TX specimen, it is 10 %.

<sup>e</sup>Zobel and van Buijtenen, 1989

<sup>f</sup>Degradable fraction in <20 mm soil-like material has been assumed to be the organic fraction as determined by volatile solids content

$$^g\text{Phase density} = \frac{\sum \text{Dry weight of each constituent in a phase}}{\sum \text{Volume of each constituent in the same phase}}$$

Table 3. Initial modelling conditions for the three MSW specimens.

Parameter	AZ	TX	CA
Volumetric moisture content, $\theta_E$ (%)	38	49	42
Solid degradable fraction (%)	24	12	9
Degradable phase density, $\gamma_{sd}$ (kg/m <sup>3</sup> )	955	1044	1338
Inert phase density, $\gamma_{si}$ (kg/m <sup>3</sup> )	1716	1727	1660

Table 4. HBM-Biodegradation calibrated model parameters for the three MSW specimens

Model parameters	Value		
	AZ	TX	CA
Initial VFA concentration, (g/m <sup>3</sup> )	8500	0	0
Initial MB concentration, (g/m <sup>3</sup> )	1200	100	10
Maximum hydrolysis rate ( $b$ ), gVFA/m <sup>3</sup> <sub>aqueous</sub> /day	6500	3500	2700
Product inhibition factor ( $k_{VFA}$ ), m <sup>3</sup> /g	1.2x10 <sup>-4</sup>	4.2x10 <sup>-4</sup>	6.3x10 <sup>-3</sup>
Structural transformation parameter ( $n$ )	1.0	0.7	0.7
Maximum specific growth rate for cellulose ( $k_0$ ), day <sup>-1</sup>	0.07	0.15	0.75
Methanogen death rate ( $k_2$ ), day <sup>-1</sup>	0.004	0.0005	0.0005
Half saturation constant ( $k_{mc}$ ), g/m <sup>3</sup>	3500	1500	700
Cell/substrate yield coefficient ( $Y$ )	0.4	0.4	0.3
Biodegradation-induced void change parameter ( $\Lambda$ )	0.8	0.7	0.8
Creep viscosity coefficient ( $\chi$ )	0.018	0.010	0.007
Reference time ( $t_{ref}$ ), day	270	220	290









